

# Old Rules in a New Game: Mapping Uncertainty Quantification to Quantum Machine Learning

Maximilian Wendlinger\*, Kilian Tscharke\*, Pascal Debus\*

\*Quantum Security Technologies

Fraunhofer Institute for Applied and Integrated Security

Garching near Munich, Germany

{maximilian.wendlinger, kilian.tscharke, pascal.debus}@aisec.fraunhofer.de

**Abstract**—One of the key obstacles in traditional deep learning is the reduction in model transparency caused by increasingly intricate model functions, which can lead to problems such as overfitting and excessive confidence in predictions. With the advent of quantum machine learning offering possible advances in computational power and latent space complexity, we notice the same opaque behavior. Despite significant research in classical contexts, there has been little advancement in addressing the black-box nature of quantum machine learning. Consequently, we approach this gap by building upon existing work in classical uncertainty quantification and initial explorations in quantum Bayesian modeling to theoretically develop and empirically evaluate techniques to map classical uncertainty quantification methods to the quantum machine learning domain. Our findings emphasize the necessity of leveraging classical insights into uncertainty quantification to include uncertainty awareness in the process of designing new quantum machine learning models.

**Index Terms**—Quantum Machine Learning, Uncertainty Quantification, Bayesian Modeling

## I. INTRODUCTION AND MOTIVATION

With the availability of large datasets, Deep Learning (DL) models have found their way into our everyday life, with the latest prominent success being Large Language Models (LLMs) solving complex tasks and responding to given questions in ways that are hardly distinguishable from human answers. As models become more complex and the computed model functions less transparent, it is hard to evaluate what underlying reasoning led to a specific model output.

In parallel, the increasing significance of quantum computers – with their high-dimensional latent Hilbert space and their power to perform complex calculations on superpositions of quantum states – has opened the path for Machine Learning (ML) models on quantum computers, or Quantum Machine Learning (QML). As a result, the last decade has seen a tremendous increase in research activity in the area of QML, both theoretically and practically (physical quantum systems scaling up to over 1000 qubits are currently being engineered [1]).

Despite this immense success in engineering and computational science, (quantum) ML models have to be *trustworthy* to be helpful in practice. As these models become more tightly integrated into applications related to the safety of human lives, it is of the greatest importance to evaluate the decisions

made by some given model in the context of the considered input data distribution. Multiple lines of research try to find interpretable characteristics of ML model output to open up this “black-box” state of current ML. One such approach is called *Uncertainty Quantification (UQ)*, which deals with the idea of quantifying the prediction confidence related to out-of-distribution (OOD) data or insufficient model complexity.

While the field of UQ in classical ML has a broad spectrum of research directions and much work is dedicated to finding solutions to the challenges described above, there is hardly any exploration of UQ in the domain of QML. Motivated by this lack of investigation, we seek to find mappings from techniques regarding UQ in classical ML to the QML context, which – as described – currently enjoys an immense research activity, due to its promising advances in many areas, such as speed-ups in tasks of computational complexity [2]–[4] and kernel optimizations using large latent spaces [5]–[7]. Thus, the main contributions of this paper are as follows:

- We construct a Bayesian QML model building upon insights from Variational Inference in QML [8] and extending this line of work by a dedicated focus on UQ.
- We design different quantum dropout methods and their relationship to Monte-Carlo (MC) dropout in classical ML, where no prior work has investigated the effects of any of the chosen methods in the given MC dropout frame.
- We extend the dropout mechanism to quantum ensembles. While initial works show how to integrate ensemble approaches into QML [8], [9], no effort has been made towards the aspects of uncertainty, a gap we fill here.
- Lastly, we explore quantum Gaussian Process (GP) models using insights from [7], [10], and extend their initial investigations by introducing UQ evaluations.
- All of the mentioned techniques above are comparatively evaluated regarding ease of implementation, quality of uncertainty estimation, and training/evaluation overhead.

## II. RELATED WORK

As described, the applications of UQ in the field of *classical* ML have been thoroughly investigated and are still topic of relevant research. An overview of recent techniques can be found in [11]–[13]. Specific details about classical UQ techniques are given in the theoretical background (Section III), along with

arXiv:2507.14919v1 [cs.LG] 20 Jul 2025

corresponding sources. In contrast, the intersection of quantum computing, machine learning, and uncertainty quantification is just beginning to be explored.

A first approach towards such an exploration is done by Park and Simeone [14], using quantum conformal prediction to augment given model outputs with “error bars” using an additional (held-out) calibration dataset. However, as the basis of their approach is the post-hoc calibration of QML circuits, the model itself is not equipped with the ability to perform predictive inference, which is the focus of this work.

From this predictive uncertainty perspective, Nguyen and Chen (2022) focus on the idea of combining the fields of QML and Bayesian learning to enhance the quantum model’s generalization performance and uncertainty estimation. To this end, the authors investigate *BayesByBackprop* and *Deep Ensembles* concerning its applicability in QML. While the authors note the positive effects of the Bayesian learning procedure on the model’s capabilities, their work lacks a dedicated evaluation of the uncertainty estimates provided by this technique, a gap we fill in this paper.

Related to our construction of MC dropout for QML, Kobayashi, Nakaji, and Yamamoto (2022) and Scala, Ceschini, Panella, and Gerace (2023) present the idea of using dropout in quantum circuit architectures. While these works focus on the regularization properties of dropout in QML, we leverage similar concepts during inference to approximate the predictive posterior distribution as done in classical UQ [17].

Lastly, as there exist many connections between QML and kernel methods, the combination of GP and QML has attracted much research interest [7], [10], [18], [19]. Once again, those works focus on the expressive power and augmentation of classical GP computations while leaving the idea of quantifying uncertainty to this present work.

### III. THEORETICAL BACKGROUND

In the following, we take a probabilistic perspective on the concepts of uncertainty in Machine Learning before introducing concepts of Quantum Machine Learning to assemble the necessary tools for the proposed mappings from classical to quantum ML.

#### A. Uncertainty in Machine Learning

As briefly introduced in Section I, UQ in ML characterizes the possibility of estimating the model confidence along with its outputs; this is of special importance for OOD data or insufficient knowledge about the data-generating process. Generally, two types of uncertainty are distinguished in the area of (Quantum) ML, differing in the underlying uncertainty source. *Aleatoric uncertainty* is intrinsic to the data-generating process and cannot be influenced by more advanced models of the system or a better understanding of the data. *Epistemic uncertainty* assumes insufficient knowledge about the data-generating process and can thus be reduced with additional information about the system. In Section V, we show how to model these uncertainties in our experiments before evaluating model predictions (visualized as confidence intervals around a learned mean function) in Section VI.

#### B. Uncertainty Quantification in Classical ML

While many approaches towards UQ in classical ML exist, we focus on four popular techniques that we later map to the quantum domain. These four techniques (Bayesian modeling, MC dropout, Ensemble methods, Gaussian Processes) are introduced in the following.

1) *Bayesian modeling*: Bayesian modeling serves as the theoretical foundation for UQ. The main idea of Bayesian modeling is as follows: Given some training data  $\mathbf{X} = \{\mathbf{x}_1, \dots, \mathbf{x}_N\}$  with associated output values  $\mathbf{Y} = \{\mathbf{y}_1, \dots, \mathbf{y}_N\}$ , we want to find model parameters  $\theta$  of a model function  $\mathbf{f}_\theta(\mathbf{x})$  that has likely generated the output [11]. Using the posterior distribution  $p(\theta|\mathbf{X}, \mathbf{Y})$  obtained from Bayes’ theorem, we can construct the predictive distribution for some unseen data sample  $\mathbf{x}^*$  via integrating over all possible parameter configurations as:

$$p(\mathbf{y}^*|\mathbf{x}^*, \mathbf{X}, \mathbf{Y}) = \int p(\mathbf{y}^*|\mathbf{x}^*\theta)p(\theta|\mathbf{X}, \mathbf{Y})d\theta, \quad (1)$$

where  $p(\theta)$  is the prior distribution over the model parameters  $\theta$  and the likelihood  $p(\mathbf{y}^*|\mathbf{x}^*\theta)$  is commonly chosen to be the softmax likelihood for classification setups and the Gaussian likelihood for regression. Due to the general intractability of the integral, a popular approximation to this posterior is done via Variational Inference [20], which seeks to minimize the Kullback-Leibler (KL) divergence between a family of parameterized distributions  $q_\lambda(\theta)$  and the posterior  $p(\theta|\mathbf{X}, \mathbf{Y})$  as

$$\lambda^* = \underset{\lambda}{\operatorname{argmin}} D_{KL}(q_\lambda(\theta)||p(\theta|\mathbf{X}, \mathbf{Y})). \quad (2)$$

Optimizing the model parameters using unbiased estimates of gradients of the cost associated with the KL divergence leads to the BayesByBackprop algorithm [21]. Together with the reparameterization trick, we obtain an easy-to-implement way of obtaining posterior distribution estimates. To further simplify the training optimization, we also generally assume the model functions to come from (independent) Gaussian distributions. In Section IV-A, we see how to map this approach to QML.

2) *Monte-Carlo dropout*: To ameliorate the computational burden of Variational Inference<sup>1</sup>, Gal and Ghahramani (2016) introduced the method of MC dropout. Their approach uses different dropout configurations for every inference pass through the neural network to obtain an ensemble of different (sparse) sub-networks. The obtained MC samples are then aggregated to obtain the mean and variance estimators of the probabilistic model.

3) *Ensemble methods*: Generalizing the notion of different sub-networks above, we can define a Deep Learning ensemble as an aggregation of several individually trained networks leading to better generalization performance and uncertainty quantification estimates. The individual models can differ in the bootstrap samples of the data set seen during training (bagging) or simply in the initial parameter configuration of

<sup>1</sup>Replacing point estimates with Gaussian mean and variance parameters doubles the number of trainable entities.

the networks [22]. Each individual network can then predict mean and variance estimators related to the input-dependent noise (aleatoric uncertainty) while the aggregation of networks includes the parameter-dependent (epistemic) noise [13].

4) *Gaussian Processes*: Generalizing the Bayesian viewpoint on neural networks and shifting from inference on latent variables to inference in function space leads to the concept of a Gaussian Process (GP). Formally, a GP is a collection of random variables, any finite number of which have a joint Gaussian distribution [23]; as such, we can define a real process  $\mathbf{f}: \mathbb{R}^D \rightarrow \mathbb{R}$  with mean function  $m(\mathbf{x})$  and covariance function  $k(\mathbf{x}, \mathbf{x}')$  as

$$m(\mathbf{x}) = \mathbb{E}[\mathbf{f}(\mathbf{x})] \quad \text{and} \quad (3)$$

$$k(\mathbf{x}, \mathbf{x}') = \mathbb{E}[(\mathbf{f}(\mathbf{x}) - m(\mathbf{x}))(\mathbf{f}(\mathbf{x}') - m(\mathbf{x}'))] \quad (4)$$

and the corresponding GP as

$$\mathbf{f}(\mathbf{x}) \sim \mathcal{GP}(m(\mathbf{x}), k(\mathbf{x}, \mathbf{x}')) \quad (5)$$

where (in the area of GP for ML) the mean function is often defined to be zero, and the shape of the functions is entirely specified by the covariance, or *GP kernel*. From this construction, we can then define the posterior (which, as a conditional of multivariate Gaussian distributions, is also a multivariate Gaussian [24]) as

$$f_* | \mathbf{X}, \mathbf{y}, \mathbf{x}_* \sim \mathcal{N}(\bar{f}_*, \mathbb{V}[f_*]), \text{ where} \quad (6)$$

$$\bar{f}_* = \mathbf{k}_*^\top [K + \sigma_\epsilon^2 \mathbf{I}]^{-1} \mathbf{y} \quad \text{and} \quad (7)$$

$$\mathbb{V}[f_*] = k(\mathbf{x}_*, \mathbf{x}_*) - \mathbf{k}_*^\top (K + \sigma_\epsilon^2 \mathbf{I})^{-1} \mathbf{k}_*, \quad (8)$$

where the kernel matrices  $K$ ,  $\mathbf{k}_*$ , and  $k(\mathbf{x}_*, \mathbf{x}_*)$  are defined as the covariances of all training points pairs, all training points and a single evaluation point, and the evaluation point with itself, respectively. For a more detailed introduction to necessary GP concepts, we refer to [23].

### C. Quantum Machine Learning

As the main goal of this paper is to establish mappings from classical to quantum ML, we need to introduce some preliminaries of the latter field. In the following, we assume basic knowledge of quantum computing and quantum gates to understand the needed concepts from QML; readers not familiar with the necessary prerequisites are referred to [25].

The basic building blocks of Quantum Machine Learning relevant in this paper are variational quantum circuits, which in turn are assembled using parametrized quantum gates. These gates (unitary operators) act on  $K$ -qubit quantum states represented as  $2^K$ -dimensional vectors of complex amplitudes. For all experiments in this paper, we focus on single-qubit rotational gates of the form

$$R(\phi, \gamma, \omega) = \begin{bmatrix} e^{-i(\phi+\omega)/2} \cos(\frac{\gamma}{2}) & -e^{i(\phi-\omega)/2} \sin(\frac{\gamma}{2}) \\ e^{-i(\phi-\omega)/2} \sin(\frac{\gamma}{2}) & e^{i(\phi+\omega)/2} \cos(\frac{\gamma}{2}) \end{bmatrix}$$

with rotational angles  $\{\phi, \gamma, \omega\}$ . These angles are used to encode the (classical) input into the quantum system by unitary operators

$$U_j(\mathbf{x}; \mathbf{w}_j, \mathbf{b}_j) = R(\mathbf{w}_j \circ \mathbf{x} + \mathbf{b}_j) \quad (9)$$

for  $\mathbf{x} \in \mathbb{R}^3$ , where the Hadamard-product parameter  $\mathbf{w}_j \in \mathbb{R}^3$  and the additive parameter  $\mathbf{b}_j \in \mathbb{R}^3$  are optimized during training. We can stack these variational gates arbitrarily for general  $\mathbf{x} \in \mathbb{R}^N$  (hence the index  $j$ ). This way, each input feature can be encoded an arbitrary number of times, accordingly called data re-upload encoding [26]. The second type of gate structure needed in the following is the two-dimensional Controlled-NOT (CNOT) gate used to entangle quantum states. Together with a final measurement process, the resulting QML model function can be written as

$$f(\mathbf{x}; \boldsymbol{\theta}) = \langle 0 | U(\mathbf{x}; \boldsymbol{\theta})^\dagger \mathcal{M} U(\mathbf{x}; \boldsymbol{\theta}) | 0 \rangle \quad (10)$$

$$= \sum_{\boldsymbol{\omega} \in \Omega} c_{\boldsymbol{\omega}} e^{i\boldsymbol{\omega}\mathbf{x}} \quad (11)$$

where Equation (10) captures the parameterized quantum circuit  $U(\mathbf{x}; \boldsymbol{\theta})$  acting on the initial zero state  $|0\rangle$  and the evaluated expectation value of the measurement observable  $\mathcal{M}$ . The importance of Equation (11) lies in the ability to write parameterized quantum circuit functions as a Fourier series whose frequency spectrum  $\Omega \subset \mathbb{R}^N$  is entirely defined by the input encoding and whose coefficients  $c_{\boldsymbol{\omega}}$  depend on the design of the circuit architecture [27]. This notation helps us to understand the idea of quantum kernels when discussing quantum Gaussian Processes in Section IV-D.

## IV. MAPPING UQ FROM ML TO QML

Given the preliminaries on Quantum Machine Learning and Uncertainty Quantification outlined above, we now turn to the combination of these fields for mapping classical UQ to variational quantum circuits.

### A. Bayesian Quantum Machine Learning

As discussed in Section II, first steps in the direction of Bayesian quantum computing are taken in [8], which are described in the following.

The essential idea is the same as in the classical Bayes-ByBackprop algorithm: As introduced in Section III-B1, we are interested in the minimization of the KL divergence from Equation (2), with the additional assumption of diagonal Gaussian distributions for the variational posterior [8]. For deterministic circuit parameters  $\boldsymbol{\theta} = \{\boldsymbol{\mu}, \boldsymbol{\rho}\}$  and parameter-free noise  $\epsilon$ , we arrive at a parameterized Gaussian distribution as  $\mathcal{N}(\boldsymbol{\mu}, \boldsymbol{\sigma}^2 = [\log(1 + \exp(\boldsymbol{\rho}))]^2)$  and resulting posterior weight samples as

$$\mathbf{w} = \boldsymbol{\mu} + \log(1 + \exp(\boldsymbol{\rho})) \circ \epsilon \quad (12)$$

where instead of classical network weights, we use the rotational angles of the quantum circuits as a basis for the construction of the variational model functions. This approach will become clear when introducing the specific quantum circuit architectures in Section V-B.

Thus, to obtain a Bayesian Quantum Machine Learning model, we iteratively evaluate the loss function

$$\mathcal{L}(x_i, y_i, \theta) = \mathcal{L}_{KL} + \mathcal{L}_{obj}, \text{ for} \quad (13)$$

$$\mathcal{L}_{KL} = \frac{1}{2} \sum_{k=1}^K (1 + \log((\sigma_k)^2) - (\mu_k)^2 - (\sigma_k)^2), \quad (14)$$

$$\mathcal{L}_{obj} = \mathcal{L}_{MSE} \text{ or } \mathcal{L}_{CE} \quad (15)$$

for multiple posterior weight samples from Equation (12) to optimize the QML model parameters  $\theta$ . The index  $k$  in Equation (14) defines the  $k$ -th element of the mean and variance vectors coming from the Gaussian prior and variational posterior [28]. As discussed in Section III-B1, we typically choose the Mean-Squared-Error (MSE) function for Gaussian likelihood objectives in regression or the Cross-Entropy (CE) for softmax likelihood classification tasks.

### B. Quantum Monte-Carlo Dropout

In classical ML, the common choice to perform dropout is to randomly select some nodes in all intermediate layers and set their output to zero. Mathematically, we can write this approach for a typical hidden layer function  $y_k = \sigma(\mathbf{W}_k \mathbf{y}_{k-1} + \mathbf{b}_k)$  of layer  $k$  (and non-linearity  $\sigma$ ) as a Hadamard product of the output with some Bernoulli vector as  $\hat{y}_k = y_k \circ z_k$ , where for each element  $z_k^{(i)}$  of  $z_k$  it holds  $z_k^{(i)} \sim \text{Bernoulli}(p)$ , given a dropout probability of  $p$ . While this approach is the most popular, many different dropout methods exist, e.g., using  $z_k^{(i)} \sim \mathcal{N}(1, \sqrt{\frac{p}{1-p}})$  for Gaussian dropout.

In a quantum circuit architecture consisting of rotational and entangling gates, we can think of similar options to introduce dropout; however, the resulting impact on the model function differs. While classical neural network structures commonly have multiple information streams from the input to the output nodes, the quantum state on which the circuit acts is influenced and modified with each dropout operation. Thus, the modification of a single gate in the circuit (e.g., dropping a rotational gate or modifying its variational parameters) changes all amplitudes of the quantum state vector, which in turn influences the measurement and observed model output.

In this light, we propose three different techniques – varying in the impact of the quantum state amplitudes – that are comparatively evaluated in Section VI, along with the other probabilistic QML models described in this work. These three techniques are as follows: First, we only drop additive parameters  $\mathbf{b}_j$  from the rotational gates as defined in Equation (9). Second, we drop whole rotation gates from the quantum circuit by replacing the specified gates with identity operators in the circuit. Last, we investigate the influence of Gaussian noise to the model parameters during each forward pass in the quantum circuit, equivalently to classical Gaussian dropout. The last variant is of particular interest as it can be represented by imperfect rotations of quantum states on the Bloch sphere, arising naturally from noise in the quantum system. For the final UQ model output, multiple forward passes through

the quantum circuit are aggregated as done in classical MC dropout, to obtain

$$\mu = \frac{1}{M} \sum_{m=1}^M \hat{y}_m \text{ and} \quad (16)$$

$$\sigma = \sqrt{\frac{1}{M-1} \sum_{m=1}^M (\hat{y}_m - \mu)^2}, \quad (17)$$

where  $M$  inference evaluations (each producing an individual model output  $\hat{y}_m$ ) are averaged for empirical mean and standard deviation estimators.

### C. Quantum Circuit Ensembles

The mechanism of using an aggregation of different models in an ensemble as described in Subsection III-B3 can be easily extended to QML, in which case multiple circuit outputs are aggregated to obtain an approximation of the posterior predictive distribution. First investigations on quantum ensembles explore the possibility of parallelism to evaluate predictions of exponentially large ensembles [9] and the quantum Bayesian approximation using deep quantum ensembles [8]. However, evaluating uncertainty estimates of quantum ensembles is a gap filled in the following.

As noted in Section III-C, the family of functions that a QML model with re-upload encoding can learn is characterized by a partial Fourier series [27], as formalized in Equation (11). Thus, all quantum circuit functions investigated in the following are periodic in nature, a property that shapes the predicted mean functions as well as the estimated confidence intervals. As done in Section IV-B, we use the empirical mean and standard deviation to aggregate the model results and obtain an approximation for the predictive posterior (see Equations (16) and (17)) for an ensemble consisting of  $M$  models, each generating an individual model output  $\hat{y}_m$ .

### D. Gaussian Processes in Quantum Machine Learning

As seen in Section III-B4, the notion of a kernel – defined by the covariance of the random variables within the GP and hence influencing the overall shape of the predictive functions – lies at the core of a Gaussian Process. Thus, we now describe how research combines GPs with *quantum kernels*.

Quantum kernels are omnipresent in the domain of QML, as they arise naturally from the feature map of the encoding of classical information into the quantum state of the system, i.e., the embedding in the (quantum) Hilbert space [6].

In general, any feature map  $\phi : \mathcal{X} \rightarrow \mathcal{F}$  from an input space  $\mathcal{X}$  to some feature space  $\mathcal{F}$  paired with the definition of an inner product on  $\mathcal{F}$  gives rise to a kernel as

$$k(x, x') := \langle \phi(x), \phi(x') \rangle_{\mathcal{F}}. \quad (18)$$

With the help of quantum circuits, we can make use of this definition and replace the classical feature map  $\phi(x)$  with a quantum embedding  $|\phi(x)\rangle$ . The resulting quantum kernel can be written as

$$k(x, x') = |\langle \phi(x') | \phi(x) \rangle|^2 = |\langle 0 | U(x')^\dagger U(x) | 0 \rangle|^2 \quad (19)$$

as shown in [7]. For the chosen re-upload encoding method in this paper, we can write the quantum kernel as

$$k(\mathbf{x}, \mathbf{x}') = \sum_{\mathbf{s}, \mathbf{t} \in \Omega} e^{i\mathbf{s}\mathbf{x}} e^{i\mathbf{t}\mathbf{x}'} c_{\mathbf{s}\mathbf{t}} \quad (20)$$

for  $\Omega \subseteq \mathbb{R}^n$  and  $c_{\mathbf{s}\mathbf{t}} \in \mathbb{C}$  [5], where for ease of notation we consider a single non-trainable upload of the data. Comparing this result to Equation (11), it is easy to see that the obtained kernel from Equation (20) is a direct consequence of the Fourier representation of the chosen quantum circuit architecture and offers an elegant way to provide a rich feature space despite the low complexity associated with the circuit structure.

## V. EXPERIMENTAL SETUP

In this section, we briefly mention the setup used for the empirical experiments in the following Section VI, including the datasets, the model architectures, and the general optimization and evaluation workflow. This allows us to have a structural baseline for both the experimental data and the architectural design of the circuits.

### A. Datasets and Pre-Processing

All models are trained and evaluated on a regression task in the main text and a classification task in Appendix C. Both datasets are kept low-dimensional to permit stable training and descriptive visualizations of uncertainty estimates. For regression, we adopt the dataset from Schuld, Sweke, and Meyer (2021), which consists of a one-dimensional Fourier series of degree two – naturally fitting the set of functions a quantum circuit can learn perfectly – as given by

$$f(x) = \sum_{n=-2}^2 c_n e^{-inx} \quad (21)$$

where the coefficients  $c_n$  allow us to modify the shape of the function. For the experiments, we use the configuration  $c_0 = 0.1$ ,  $c_1 = c_2 = 0.15 - 0.15i$  and the fact that  $c_{-k} = c_k^*$ , leading to the function shown as a dashed line in Figure 1.

To estimate the uncertainty of the models, we construct two adapted versions of this regression setup: First, we include a gap for  $x_i \in [\pi, 1.6\pi)$  (epistemic uncertainty). Second, we include a gap for  $x_i \in [1.4\pi, 2\pi)$  and sample from the modified function

$$f_\varepsilon(x) = f(x) + \varepsilon \quad \text{for } \varepsilon \sim \mathcal{N}(0, \sigma_\varepsilon^2) \quad (22)$$

with  $\sigma_\varepsilon = 0.1$  to include aleatoric uncertainty. Both versions of the dataset are visualized in Figure 1, where the individual training data points are depicted as gray circles.

For classification, the popular two-moons<sup>2</sup> dataset serves as the benchmark for empirical experiments as it enables clear visualization of the non-linear decision boundary while being low-dimensional enough to work within the QML regime. See Appendix C for all classification experiments.

<sup>2</sup>[https://scikit-learn.org/stable/modules/generated/sklearn.datasets.make\\_moons.html](https://scikit-learn.org/stable/modules/generated/sklearn.datasets.make_moons.html)

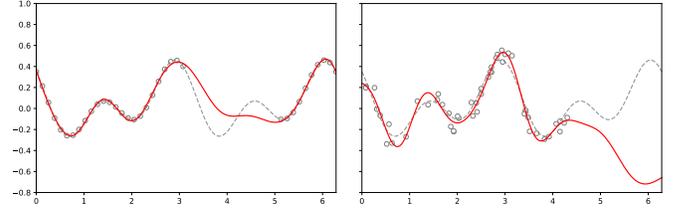


Fig. 1: Regression functions representing epistemic-only uncertainty (left) and a combination of aleatoric and epistemic uncertainty (right). In red, the output of a deterministic QML model is given, showing its inability to adhere to the correct periodicity of the underlying data function when noise is present in the system.

### B. Quantum Machine Learning Architectures

Although the individual mappings from classical to quantum UQ differ dramatically by design, where, e.g., ensemble methods are a mixture of different base models and MC dropout employs a single model with different dropout configurations (and GP models have a different basis for modeling the data distribution altogether), we try to keep a similar structure for all (base-) models. Doing so allows us to compare the uncertainty estimates more effectively, using a common structural ground. This basic architecture consists of six rotational layers in a single-qubit quantum circuit followed by a calculation of the expected value of a measurement in the Pauli-Z basis<sup>3</sup>. The circuit is given in Figure 2. To adjust the univariate data

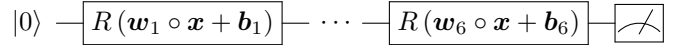


Fig. 2: The basic architecture for all quantum models, on which the different mappings from classical to quantum UQ are developed and evaluated.

input to the rotational parameter vectors, we stack the input into three-tuples as  $\mathbf{x} = (x, x, x)$ . The main idea behind this architecture is the relationship to the proposed regression and classification tasks, where the chosen model design showed a good trade-off between the ability to fit target functions despite the use of dropout (or other UQ techniques) and possible overfitting scenarios.

The training procedure of the models follows best practices from classical and quantum ML, where the described quantum circuit ansatz is optimized using the Adam optimization scheme [29] with a learning rate of  $\eta = 0.01$ , an upper bound of 1000 training epochs and early stopping cutoffs at  $\mathcal{L}_{MSE} < 0.005$  for regression and  $\mathcal{L}_{CE} < 0.3$  for classification. More details about the model architecture, optimization process, and evaluation can be found in Appendix A.

<sup>3</sup>This means that the QML model output is bounded by  $f(\mathbf{x}; \theta) \in [-1, 1]$  by definition of expectation values [25].

## VI. EMPIRICAL EVALUATION

With the tools assembled throughout this work, we now describe the outcomes of applying UQ techniques from Section IV to typical QML model architectures as constructed in Section V. After qualitative empirical results for each model are shown, we introduce the measure of calibration error and comparatively evaluate all architectures.

### A. Qualitative Analysis

For qualitative analysis, we visualize the predictive output distribution for each of the proposed quantum UQ models, including a Bayesian quantum circuit, three MC dropout models (bias-only, rotation, Gaussian dropout), a quantum circuit ensemble and a GP equipped with a quantum kernel. In each case, we plot the mean output function and shade the area containing one and two standard deviations, respectively.

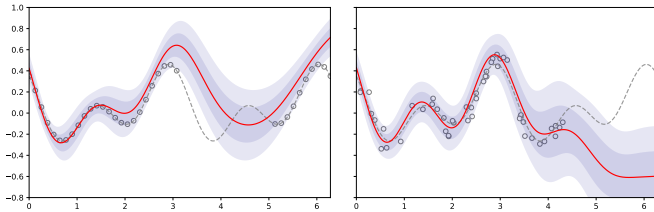


Fig. 3: Results for a Bayesian QML model for a noiseless (left) and a noisy regression task (right).

First, we show the results for Bayesian QML regression, where we use the six-layer architecture in combination with the Bayesian framework and the re-parameterization trick as described in Section IV-A. Figure 3 shows the resulting model outputs for both regression scenarios (epistemic only versus epistemic and aleatoric uncertainty). In both cases, the model cannot fully capture the function shape once data samples are missing but reflects this uncertainty in larger deviation bounds within the respective regions. While epistemic uncertainty is reflected in the predictive variance estimators, the posterior-pushforward modeling [13] cannot truthfully capture aleatoric uncertainty.

Next, we investigate quantum MC dropout by evaluating all chosen dropout configurations (bias-only, rotation, Gaussian dropout) as shown in Figure 4. More precisely, we use the same architecture as before and apply a dropout rate of  $p = 0.1$  to the dropout algorithms described in Section IV-B. While all models show uncertainty in regions of training data absence, the models differ in their predicted variance: Bias dropout leads to relatively tight uncertainty bounds, especially in the noisy regression setting. Rotation dropout poses a more significant structural burden for each inference pass, leading to larger confidence intervals. Gaussian dropout shows the best visual results, given the slight changes in rotation angles due to Gaussian noise. As before, the predictive distributions only capture epistemic uncertainty.

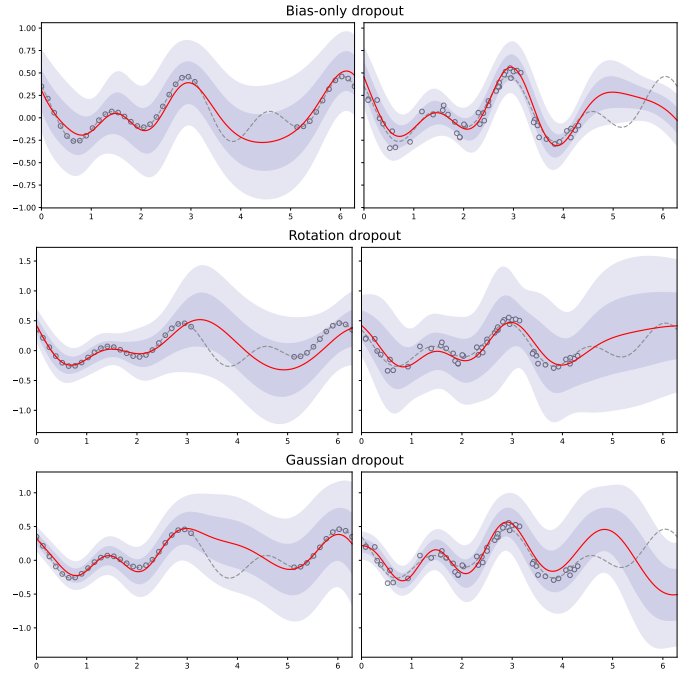


Fig. 4: Regression results for all MC dropout QML models.

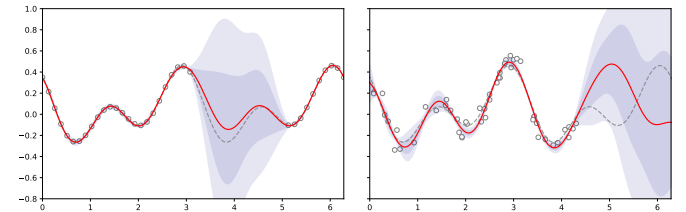


Fig. 5: Regression results for an ensemble of QML models.

For ensembles, this behavior changes. When aggregating eight individual QML model outputs to form mean and standard deviation estimators, the ability to represent epistemic and aleatoric uncertainty emerges, as seen in Figure 5. Intuitively, the confidence shapes align well with the underlying problem statement, where a near-perfect fit is achieved in regions of sufficient data, and significant deviations from the mean function emerge in the absence of data samples.

Last, we study the uncertainty estimates given by Gaussian Process regression using a quantum kernel, as visualized in Figure 6. The mathematical structure of the GP allows perfectly capturing noiseless data samples (left subfigure) and adapting to aleatoric uncertainty by incorporating the noise into the covariance matrices. The high-frequency structure of the employed quantum kernel leads to relatively large uncertainty bounds between samples, even in regions of higher data density. The uncertainty shapes associated with different underlying kernel circuit structures are investigated in Appendix B.

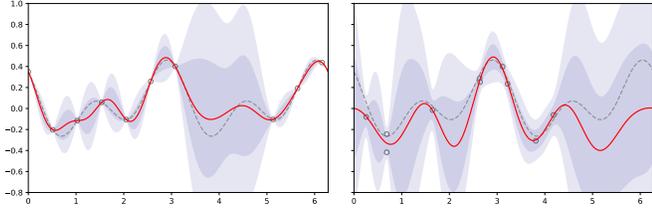


Fig. 6: Gaussian Process regression results using a quantum re-upload encoding kernel consisting of two qubits and two layers.

### B. Quantitative Analysis

For a more rigorous evaluation, we introduce the notation of the *Expected Calibration Error (ECE)* [30] as the expected difference between the model’s confidence and accuracy. If we plot the observed confidence (actual model output accuracy within some confidence interval) on the y-axis against the expected confidence (expected number of samples to lie within that interval) on the x-axis, we obtain the calibration curves as shown in Figure 7, where larger deviations from the diagonal express larger miscalibration [31]. To obtain the ECE, we

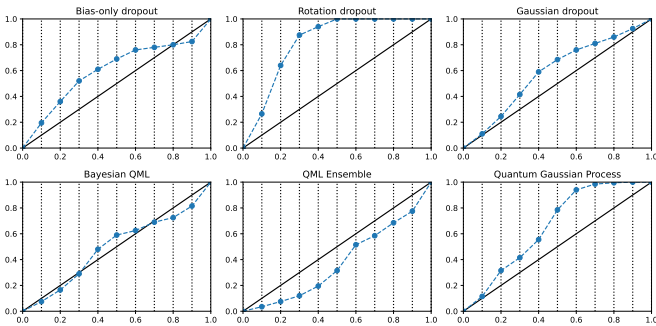


Fig. 7: Calibration curves for all models investigated in this paper. Large deviations from the diagonal indicate poor calibration, where lines over (under) the diagonal signal underconfidence (overconfidence).

then take the mean absolute distance between the curves for each of the chosen confidence intervals (in Figure 7, there are 11 confidence intervals, ranging from 0 to 100%). Together with insights from individual model implementations, we summarize the results from the quantitative analysis in Table I.

First, we note the mere possibility of mapping UQ methods from classical ML to QML. Since the underlying model functions differ between classical and quantum ML and we have a much more complex embedding space when working on qubits instead of classical bits, it is by no means trivial to infer that the chosen classical techniques are applicable in QML as well as they proved to be. Even more so, given the empirical evaluation, it becomes clear that different methods have different properties of computational requirements,

quality of uncertainty predictions, and ease of integration into existing QML architectures. Out of all models, the Bayesian QML framework shows the best calibration; however, during the empirical evaluations, we found that even slight modifications of circuits, such as Gaussian noise influences for quantum MC dropout, results in well-calibrated QML models with a trivial implementation overhead. Our implementation of quantum ensembles was the only technique that shows *overconfidence* in the model predictions. In contrast, dropout and GP models are slightly *underconfident*. In safety-critical scenarios, this behavior is better aligned with the intention of uncertainty quantification; however, we find that in any case, the underlying circuit architecture needs to be adapted to the specific use-case.

TABLE I: Findings of comparative evaluation for all models, including the ECE, computational cost, and quality of uncertainty.

Model	ECE	Cost	Quality
Bayesian QML	0.0395	Medium	High
Bias-only MC d.	0.1082	Low	Low-Med.
Rotation MC d.	0.2927		
Gaussian MC d.	0.0818		
QML Ens.	0.1091	Medium	Medium
Quantum GPs	0.1459	High	Medium

## VII. SUMMARY AND OUTLOOK

In this work, we extend foundations on quantum Bayesian modeling, quantum kernels, and ensemble theory to the applications of quantum UQ. Furthermore, we develop new ideas of bridging MC dropout techniques to QML, building upon their potential in classical ML. The resulting model calibration is comparatively evaluated for all proposed approaches, first qualitatively via deviation bounds and quantitatively via calibration metrics.

The empirical results indicate the potential of UQ in QML. Most strikingly, a Bayesian approach to QML model optimization (or a similar noise-centric viewpoint via Gaussian dropout) provides a good trade-off between implementation complexity and quality of uncertainty prediction. While we shed light on multiple possible extensions at the intersection of UQ and QML, many avenues are yet to be explored, where we mention the extension to more complex scenarios as well as the inclusion of further UQ techniques here and give a more detailed overview of limitations and future work in Appendix D.

Incorporating insights into the field of Uncertainty Quantification in the context of QML is an important – but often overlooked – step when developing quantum algorithms, as we see quantum hardware become increasingly powerful and quantum algorithms increasingly complex. In line with the principle of “security by design,” we should therefore integrate trustworthiness into QML from the outset to avoid encountering the same issues as faced in classical ML approaches.

## REFERENCES

- [1] Jay Gambetta, *The hardware and software for the era of quantum utility is here*, Dec. 2023. (visited on 10/16/2024).
- [2] P. Shor, “Algorithms for quantum computation: Discrete logarithms and factoring,” in *Proceedings 35th Annual Symposium on Foundations of Computer Science*, Santa Fe, NM, USA: IEEE Comput. Soc. Press, 1994, pp. 124–134, ISBN: 978-0-8186-6580-6. DOI: 10.1109/SFCS.1994.365700. (visited on 10/18/2024).
- [3] A. W. Harrow, A. Hassidim, and S. Lloyd, “Quantum algorithm for solving linear systems of equations,” *Physical Review Letters*, vol. 103, no. 15, p. 150502, Oct. 2009, ISSN: 0031-9007, 1079-7114. DOI: 10.1103/PhysRevLett.103.150502. arXiv: 0811.3171 [quant-ph]. (visited on 08/26/2024).
- [4] Y. Liu, S. Arunachalam, and K. Temme, “A rigorous and robust quantum speed-up in supervised machine learning,” *Nature Physics*, vol. 17, no. 9, pp. 1013–1017, Sep. 2021, ISSN: 1745-2473, 1745-2481. DOI: 10.1038/s41567-021-01287-z. arXiv: 2010.02174 [quant-ph]. (visited on 09/03/2024).
- [5] M. Schuld, *Supervised quantum machine learning models are kernel methods*, Apr. 2021. DOI: 10.48550/arXiv.2101.11020. arXiv: 2101.11020 [quant-ph, stat]. (visited on 10/03/2024).
- [6] M. Schuld and N. Killoran, “Quantum machine learning in feature Hilbert spaces,” *Physical Review Letters*, vol. 122, no. 4, p. 040504, Feb. 2019, ISSN: 0031-9007, 1079-7114. DOI: 10.1103/PhysRevLett.122.040504. arXiv: 1803.07128 [quant-ph]. (visited on 10/01/2024).
- [7] F. Rapp and M. Roth, “Quantum Gaussian Process Regression for Bayesian Optimization,” *Quantum Machine Intelligence*, vol. 6, no. 1, p. 5, Jun. 2024, ISSN: 2524-4906, 2524-4914. DOI: 10.1007/s42484-023-00138-9. arXiv: 2304.12923 [quant-ph]. (visited on 07/09/2024).
- [8] N. Nguyen and K.-C. Chen, “Bayesian Quantum Neural Networks,” *IEEE Access*, vol. 10, pp. 54110–54122, 2022, ISSN: 2169-3536. DOI: 10.1109/ACCESS.2022.3168675. (visited on 09/10/2024).
- [9] M. Schuld and F. Petruccione, *Quantum ensembles of quantum classifiers*, Apr. 2017. DOI: 10.48550/arXiv.1704.02146. arXiv: 1704.02146 [quant-ph, stat]. (visited on 09/18/2024).
- [10] Z. Zhao, A. Pozas-Kerstjens, P. Rebenrost, and P. Wittek, “Bayesian Deep Learning on a Quantum Computer,” *Quantum Machine Intelligence*, vol. 1, no. 1-2, pp. 41–51, May 2019, ISSN: 2524-4906, 2524-4914. DOI: 10.1007/s42484-019-00004-7. arXiv: 1806.11463 [quant-ph, stat]. (visited on 07/09/2024).
- [11] Y. Gal, “Uncertainty in Deep Learning,” Ph.D. dissertation, University of Cambridge, Sep. 2016.
- [12] W. He, Z. Jiang, T. Xiao, Z. Xu, and Y. Li, *A Survey on Uncertainty Quantification Methods for Deep Learning*, Jul. 2024. arXiv: 2302.13425 [cs, stat]. (visited on 10/08/2024).
- [13] V. Nemani *et al.*, “Uncertainty Quantification in Machine Learning for Engineering Design and Health Prognostics: A Tutorial,” *Mechanical Systems and Signal Processing*, vol. 205, p. 110796, Dec. 2023, ISSN: 08883270. DOI: 10.1016/j.ymssp.2023.110796. arXiv: 2305.04933 [cs]. (visited on 07/09/2024).
- [14] S. Park and O. Simeone, *Quantum Conformal Prediction for Reliable Uncertainty Quantification in Quantum Machine Learning*, Oct. 2023. arXiv: 2304.03398 [quant-ph]. (visited on 07/09/2024).
- [15] M. Kobayashi, K. Nakaji, and N. Yamamoto, “Overfitting in quantum machine learning and entangling dropout,” *Quantum Machine Intelligence*, vol. 4, no. 2, p. 30, Dec. 2022, ISSN: 2524-4906, 2524-4914. DOI: 10.1007/s42484-022-00087-9. arXiv: 2205.11446 [quant-ph]. (visited on 08/28/2024).
- [16] F. Scala, A. Ceschini, M. Panella, and D. Gerace, “A General Approach to Dropout in Quantum Neural Networks,” *Advanced Quantum Technologies*, p. 2300220, Dec. 2023, ISSN: 2511-9044, 2511-9044. DOI: 10.1002/qute.202300220. arXiv: 2310.04120 [quant-ph]. (visited on 08/28/2024).
- [17] Y. Gal and Z. Ghahramani, “Dropout as a Bayesian Approximation: Representing Model Uncertainty in Deep Learning,” no. arXiv:1506.02142, Oct. 2016. arXiv: 1506.02142 [cs, stat]. (visited on 07/30/2024).
- [18] N. Polson, V. Sokolov, and J. Xu, *Quantum Bayesian Computation*, Mar. 2023. arXiv: 2208.08068 [cs, math, stat]. (visited on 07/09/2024).
- [19] Z. Zhao, J. K. Fitzsimons, and J. F. Fitzsimons, “Quantum assisted Gaussian process regression,” *Physical Review A*, vol. 99, no. 5, p. 052331, May 2019, ISSN: 2469-9926, 2469-9934. DOI: 10.1103/PhysRevA.99.052331. arXiv: 1512.03929 [quant-ph, stat]. (visited on 07/09/2024).
- [20] M. I. Jordan, Z. Ghahramani, T. S. Jaakkola, and L. K. Saul, “An introduction to variational methods for graphical models,” *Machine learning*, vol. 37, pp. 183–233, 1999.
- [21] C. Blundell, J. Cornebise, K. Kavukcuoglu, and D. Wierstra, *Weight Uncertainty in Neural Networks*, May 2015. DOI: 10.48550/arXiv.1505.05424. arXiv: 1505.05424 [cs, stat]. (visited on 09/10/2024).
- [22] B. Lakshminarayanan, A. Pritzel, and C. Blundell, “Simple and Scalable Predictive Uncertainty Estimation using Deep Ensembles,” no. arXiv:1612.01474, Nov. 2017. DOI: 10.48550/arXiv.1612.01474. arXiv: 1612.01474 [cs, stat]. (visited on 09/25/2024).
- [23] Carl Edward Rasmussen, “Gaussian Processes in Machine Learning,” in *Advanced Lectures on Machine Learning*, vol. 3176, 2004.

- [24] K. P. Murphy, *Probabilistic Machine Learning: An Introduction* (Adaptive Computation and Machine Learning Series). Cambridge, Massachusetts: The MIT Press, 2022, ISBN: 978-0-262-04682-4.
- [25] M. A. Nielsen and I. L. Chuang, *Quantum Computation and Quantum Information*, 10th anniversary ed. Cambridge ; New York: Cambridge University Press, 2010, ISBN: 978-1-107-00217-3.
- [26] A. Pérez-Salinas, A. Cervera-Lierta, E. Gil-Fuster, and J. I. Latorre, *Data re-uploading for a universal quantum classifier*, <https://arxiv.org/abs/1907.02085v3>, Jul. 2019. DOI: 10.22331/q-2020-02-06-226. (visited on 10/03/2024).
- [27] M. Schuld, R. Sweke, and J. J. Meyer, “The effect of data encoding on the expressive power of variational quantum machine learning models,” *Physical Review A*, vol. 103, no. 3, p. 032430, Mar. 2021, ISSN: 2469-9926, 2469-9934. DOI: 10.1103/PhysRevA.103.032430. arXiv: 2008.08605 [quant-ph, stat]. (visited on 07/10/2024).
- [28] D. P. Kingma and M. Welling, “Auto-Encoding Variational Bayes,” Dec. 2013. (visited on 09/12/2024).
- [29] D. P. Kingma and J. Ba, “Adam: A Method for Stochastic Optimization,” no. arXiv:1412.6980, Jan. 2017. arXiv: 1412.6980 [cs]. (visited on 10/05/2024).
- [30] M. Pakdaman Naeni, G. Cooper, and M. Hauskrecht, “Obtaining Well Calibrated Probabilities Using Bayesian Binning,” *Proceedings of the AAAI Conference on Artificial Intelligence*, vol. 29, no. 1, Feb. 2015, ISSN: 2374-3468, 2159-5399. DOI: 10.1609/aaai.v29i1.9602. (visited on 10/08/2024).
- [31] V. Kuleshov, N. Fenner, and S. Ermon, “Accurate Uncertainties for Deep Learning Using Calibrated Regression,” no. arXiv:1807.00263, Jul. 2018. arXiv: 1807.00263 [cs]. (visited on 10/11/2024).
- [32] A. Paszke *et al.*, *PyTorch: An Imperative Style, High-Performance Deep Learning Library*, Dec. 2019. arXiv: 1912.01703 [cs, stat]. (visited on 10/05/2024).
- [33] V. Bergholm *et al.*, *PennyLane: Automatic differentiation of hybrid quantum-classical computations*, Jul. 2022. arXiv: 1811.04968 [physics, physics:quant-ph]. (visited on 10/04/2024).
- [34] J. Z. Liu *et al.*, *Simple and Principled Uncertainty Estimation with Deterministic Deep Learning via Distance Awareness*, Oct. 2020. arXiv: 2006.10108 [cs, stat]. (visited on 07/09/2024).
- [35] J. Z. Liu *et al.*, *A Simple Approach to Improve Single-Model Deep Uncertainty via Distance-Awareness*, Dec. 2022. arXiv: 2205.00403 [cs, stat]. (visited on 07/12/2024).
- [36] D. P. Kingma, T. Salimans, and M. Welling, “Variational Dropout and the Local Reparameterization Trick,” no. arXiv:1506.02557, Dec. 2015. DOI: 10.48550/arXiv.1506.02557. arXiv: 1506.02557 [cs, stat]. (visited on 09/28/2024).

APPENDIX A  
MODEL OPTIMIZATION AND EVALUATION

As stated in the main text, the basic optimization and evaluation procedure used in the empirical evaluations in Section VI are designed following best practices from classical and quantum ML. First, the described quantum circuit ansatz consisting of six re-upload encoding layers and one qubit is evaluated on a set of training points to compute the value of a chosen loss function. For regression experiments, we make use of the mean-squared error function<sup>4</sup>, whereas the binary cross-entropy function<sup>5</sup> serves as a basis for classification optimization. The gradient of the chosen loss function is then used to update the model parameters, using the Adam [29] algorithm, where a learning rate of  $\eta = 0.01$  is used for standard model optimization. For models that use aggregation, such as dropout or ensemble circuits, we use ten forward passes through the model to estimate the predictive mean in each training step and 1000 model evaluations on the test set to produce the figures in Section VI-A. For the Bayesian treatment of QML using BayesByBackProp, we substitute the standard loss functions with Equation (13) as derived in Section IV-A. For the GP, it was found during training, that the basic one-qubit six-layer architecture leads to instabilities during training, and we switched the underlying quantum circuit kernel to an architecture consisting of two qubits and two layers (see AppendixB).

All models are trained until convergence on the regression and classification datasets. That is, we have an upper bound of 1000 epochs for all models, with an early stopping cutoff if the mean-squared error loss falls below a threshold of  $\mathcal{L}_{MSE} < 0.005$  for regression or if the binary cross-entropy is  $\mathcal{L}_{CE} < 0.3$  for classification.

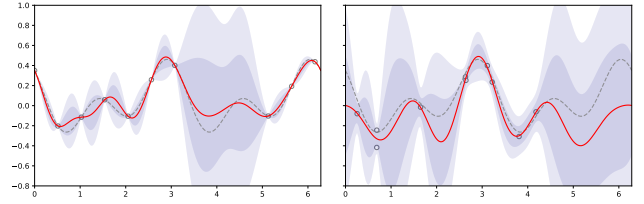
The quantum model and optimization routines are implemented on a PyTorch [32] state-vector simulator based on the PennyLane [33] *StronglyEntanglingLayers*<sup>6</sup> template for the possibility of integration into existing ML pipelines and efficient gradient evaluation. Note that no entanglement is required for one qubit, and the *StronglyEntanglingLayers* template collapses to repeated rotational layers where we incorporate the input for re-upload encoding, as shown in Equation (9). For the quantum kernel GP algorithms, we utilize the scikit-learn library<sup>7</sup>.

APPENDIX B  
GAUSSIAN PROCESS REGRESSION FOR DIFFERENT  
RE-UPLOADING CONFIGURATIONS

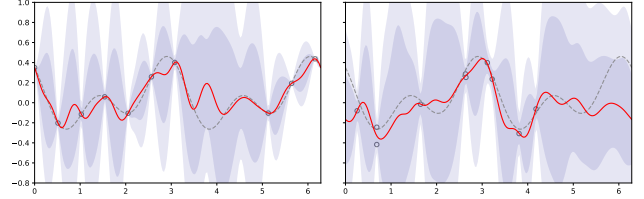
During the experiments with quantum GP regression in Section VI-A, we noted the dependency of the resulting output functions on the underlying kernel. More specifically, we

<sup>4</sup><https://pytorch.org/docs/stable/generated/torch.nn.MSELoss>  
<sup>5</sup><https://pytorch.org/docs/stable/generated/torch.nn.BCEWithLogitsLoss>  
<sup>6</sup><https://docs.pennylane.ai/en/stable/code/api/pennylane.StronglyEntanglingLayers>  
<sup>7</sup>[https://scikit-learn.org/stable/modules/gaussian\\_process](https://scikit-learn.org/stable/modules/gaussian_process)

obtained drastically different mean function shapes and confidence intervals in the evaluations by changing the number of re-upload encoding layers for our chosen circuit architecture.



(a) Quantum Gaussian Process regression output for shallow circuit kernel.



(b) Quantum Gaussian Process regression output for deep circuit kernel.

Fig. 8: Comparative overview over regression output functions showing the influence of the underlying circuit complexity.

As a baseline, we again visualize the quantum GP regression plots (here: Figure 8a) from the empirical evaluation, where we employ a two-qubit, two-layer quantum circuit architecture.

If we increase the number of layers to obtain a two-qubit, six-layer case (which is still relatively low-scale compared to typical circuit architectures in the range of  $10 - 10^3$  layers), we obtain the GP model output depicted in Figure 8b. We can see the difference in the mean function, showing a behavior typical for overfitting, with large fluctuations in the intervals between data points. Also, the uncertainty bounds between neighboring data points scale up dramatically, leading to an overestimation of the model’s uncertainty.

The shape of the mean and deviation bounds are a result of the Fourier series nature of the underlying circuit kernel, where additional layers introduce higher frequencies into the spectrum of the sum. Therefore, we again stress the importance of finding suitable hyper-parameters and fitting the chosen model to the underlying task, as small differences in the model architecture can lead to large differences in the resulting uncertainty quality as shown in Figure 8.

APPENDIX C  
CLASSIFICATION RESULTS

In the following, we give the results for all mentioned models on the classification experiments. More specifically, for each approach (Bayesian QML, [Bias-only, Rotation, Gaussian]- MC dropout, quantum ensemble, quantum GP), we first evaluate the predictive performance as signaled by the class scores. Second, we also plot the predictive uncertainty for the output space, as given by the predicted variance. For an example, see the output scores for Bayesian QML in Figure 10.

Before evaluating the UQ capabilities of all models, we show the classification output of a deterministic QML model in Figure 9. As we can see, a periodic output pattern emerges that perfectly fits the training samples but includes many areas of high class-probabilities despite the lack of data in these regions.

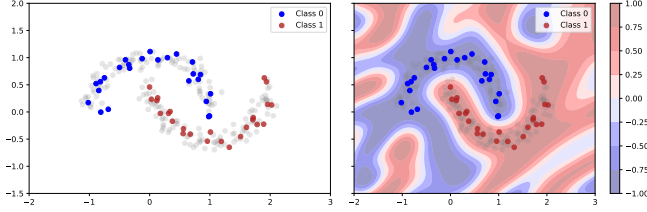


Fig. 9: Classification results for deterministic QML model using one-qubit six-layer reupload encoding architecture.

Given this behavior as a baseline to improve, we first investigate the classification output of Bayesian QML in Figure 10. Compared to the outcome of a deterministic QML circuit without UQ capabilities we see a much smoother landscape. Additionally, from the plot on the right, we can convince

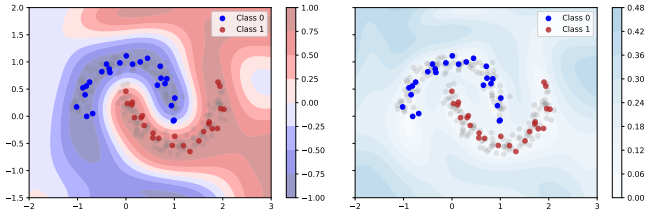


Fig. 10: Classification results for a Bayesian QML model. Left: Class prediction scores. Right: Predicted model uncertainty (standard deviation) as derived in Section IV-A.

ourselves of the basic UQ properties of the Bayesian QML output, where the standard deviation of the predictive posterior is visualized as blue shades of increasing opacity. In contrast to a simple classification output giving class scores for ‘0’ or ‘1’, the Bayesian treatment of the classifier allows an estimate of uncertainty for each data point, depending on the relative position to the training points and the output function<sup>8</sup>.

For quantum MC dropout, we visualize the classification output in Figure 11. First, we can note that the overall output shape of the classification scores is similar between the models (and also with respect to the other models used in the UQ experiments), but much smoother than the deterministic baseline from Figure 9. However, we see some differences when investigating in more detail: As in the regression setting, we notice that the uncertainty scale of the models differs (as seen on the right subplots of each row in Figure 11), where the rotation dropout model has large regions with standard

<sup>8</sup>Note that the underlying QML model is limited to Fourier series functions after all, so we cannot completely eliminate periodicity in the output.

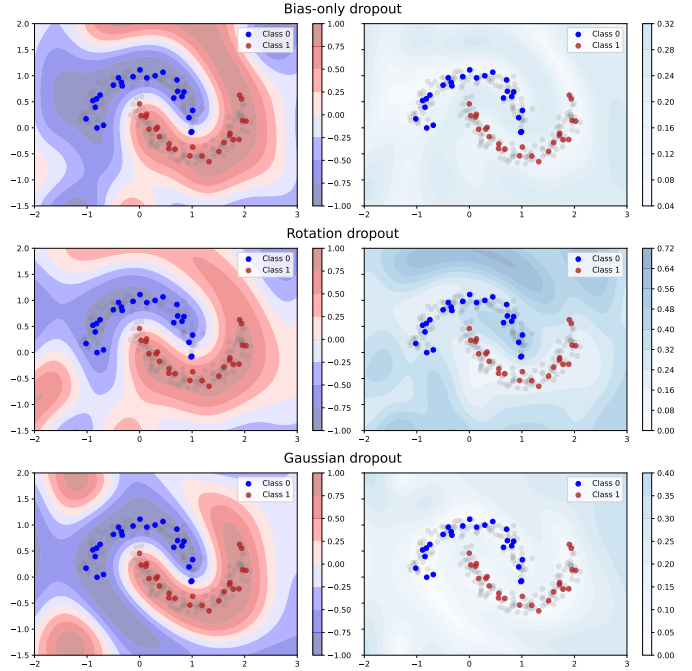


Fig. 11: Classification results for three different approaches to MC dropout in QML.

deviations up to 0.7, whereas the maximum of the other models is around  $\sigma = 0.35$ . A region of interest is the center of the scatter plot, around the position  $(x_1, x_2) = (1, 0)$ , where class ‘0’ (blue) has its right lower tail. In this region, we can see that the rotation dropout has large uncertainty values, even though we have data samples in the training set, a behavior not seen as pronounced in the other two models. Last, regardless of the employed dropout mechanism, we cannot fully eliminate the periodic output of the QML classifier, but the dropout averaging scheme helps to smooth out the diverse individual outputs, such that we have only few regions with both a definite class prediction (dark red or blue areas on the left subplot) and a low variance (white region in the right subplot).

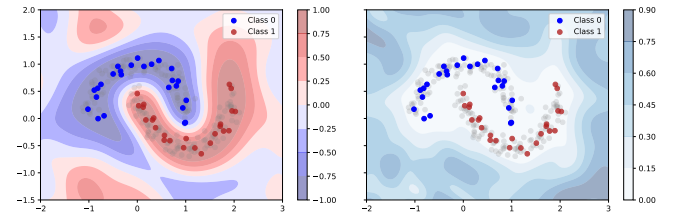


Fig. 12: Classification results for an ensemble of eight quantum classifiers using empirical mean and standard deviation to aggregate the outputs.

For quantum ensembles (more specifically, the aggregation of eight quantum circuits as used in the regression setting), the classification scores and uncertainty predictions are depicted in Figure 12. While the main class prediction shapes are similar

to the methods presented before, two characteristics stand out. On the left plot, we see a comparatively large area shaded in very light tones, indicating an indifferent model output for class predictions far away from observed data points, which already provides some insight into the model’s calibration without considering the uncertainty prediction itself. In the right plot, we find that the uncertainty of the model is low in the entire center region, regardless of the class boundaries. This quality presents the difference between ensemble circuits and the other methods discussed here: In regions where many data points are present, the individual model predictions will match almost perfectly, and we obtain very strong confidence values in the model (which also leads to a model calibration that is oriented towards overconfidence – as seen in Figure 7). In contrast to circuit ensembles, we do not expect this phenomenon to appear as pronounced, e.g., in MC dropout circuits, as each new dropout configuration leads to a new circuit configuration and quantum state resulting in a slightly different output, even in high-density data regions.

Last, we examine the quantum GP classification model, using the same two-qubit, two-layer kernel as in the regression case. To this end, we make use of scikit-learn’s `GaussianProcessClassifier`<sup>9</sup>, which in turn incorporates a logistic link function into the underlying GP model, thus mapping the outputs to the range  $\hat{y}_k \in [0, 1]$ . This architecture leads to uncertainty estimates in the class scores but does not allow to explicitly return the uncertainty values as in the approaches before, hence we only show the GP class scores in Figure 13.

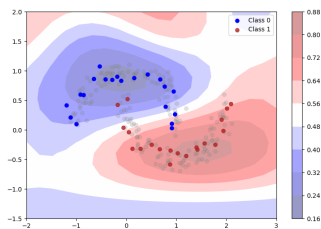


Fig. 13: Classification results for a Gaussian Process with a quantum kernel consisting of two qubits and two layers.

As seen in the output landscape, the given quantum kernel is not complex enough to obtain the two-moon shape for a perfect data fit. While most points are classified correctly and we find areas of large uncertainty (as shown by regions shaded in white), a similar periodic output pattern like the ones discussed in other classification plots emerges.

#### APPENDIX D LIMITATIONS AND FUTURE WORK

Building upon some of the limitations already mentioned in the main text, we first note the limitation of only integrating a comparatively small subset of the multitude of possible

<sup>9</sup>[https://scikit-learn.org/dev/modules/generated/sklearn.gaussian\\_process.GaussianProcessClassifier.html](https://scikit-learn.org/dev/modules/generated/sklearn.gaussian_process.GaussianProcessClassifier.html)

approaches to UQ presented in the field of classical ML. To give some examples which we find interesting but considered to be out of scope for this work, we mention a list of three possible extensions:

- The theory of obtaining uncertainty predictions from deterministic networks gains much attention in classical ML and presents itself suitable for integrating into QML. Most prominently, Spectral-Normalized Gaussian Processes seek to enforce a bi-Lipschitz condition on the latent model space to obtain distance-awareness [34], [35]. Mapping this approach to QML with its large latent space can be an interesting topic for future work.
- Variational MC dropout, an extension of the Gaussian dropout case which incorporates adaptive dropout rates into the model [36], may lead to even better results and adaptability as the discussed MC dropout methods evaluated here. As we have already seen the nice integration of dropout to QML, this may also be an example of a good symbiosis for future insights.
- Lastly, the combination of different approaches, as briefly mentioned when discussing quantum ensembles (and the possibility of integrating probabilistic outputs into each sub-model within the ensemble), is also an interesting topic that might lead to better results for some use cases and underlying data distributions.

Another main limitation, also stemming from the fact that we currently only have limited expressive power in the QML circuit architectures, is the focus on low-dimensional datasets. While the used data distribution (one-dimensional trigonometric regression and the two-moons classification) allows meaningful visualizations of the model predictions and uncertainty estimates, we must transfer these findings to more advanced, real-world examples before being able to evaluate the model architectures in practice. As a first step, it may be sensible to increase the dimensionality slightly, e.g., using image classification and higher-dimensional regression functions. Parallel to the importance of finding different evaluation datasets, it is essential to vary the underlying QML model and scale up the used circuit architecture to more qubits and layers to explore if insights from this work also hold in more complex scenarios.

#### APPENDIX E CODE AVAILABILITY

All implemented model architectures and their respective results on the chosen datasets are made available upon reasonable request.